4 Ultra-shallow Shear-wave Reflections Locating Near-surface Buried Structures in the Unexcavated Southern Fringe of the Ancient Ostia, Rome

Ranajit Ghose,[1] Jianhuan Liu,[1] Deyan Draganov,[1,3] Dominique Ngan-Tillard,[1,3] Martijn Warnaar,[1] Joeri Brackenhoff,[1] Jens van den Berg[1], and Hanna Stöger†[2]

[1] Department of Geoscience and Engineering, Delft University of Technology, The Netherlands
[2] Faculty of Archaeology, Leiden University, The Netherlands
[3] Leiden Delft Erasmus Centre for Global Heritage and Development, The Netherlands

The southern boundary of Region IV of ancient Ostia coincides with the southern limit of the excavated area of the ancient city. The perceived expanse of the city is influenced by the extent of the excavation. It is not known whether the unexcavated part lying south of Region IV also contains structures of antiquity which might have important historical significance. We have carried out high-resolution, shallow seismic reflection surveys along two profiles, using shear (transverse) waves. The goal of these pilot surveys was to see whether any indication of ultra-shallow scatterers, indicating the potential location of shallow-buried structures, can be found in the shear-wave data. The results show very distinct back-scattered shear-wave arrivals from a mysterious tumulus, whose location along Line A was known. It has been possible to interpret with reasonable confidence the location of several conspicuous, shallow scatterers in the two seismic profiles. Use of shear waves and a high-frequency, electromagnetic shear-wave vibrator was crucial to achieving seismic resolution of nearly 25 cm. The amplitude of the scattered energy is helpful to locate the relatively strong scatterers. Our results suggest that the unexcavated areas located south of Region IV most likely contain buried underground structures. 3-D shear-wave seismic reflections together with new seismic-imaging approaches will be promising to illuminate the unknown shallow subsurface of this important archaeological site in a non-invasive manner.

4.1 INTRODUCTION

The archaeological site of Ostia, the important harbour city of ancient Rome, presents impressive, well-preserved architectural remains that shed light on the complexity of the Roman urban life of antiquity. Ancient Ostia was situated about 25 km west of Rome, at the mouth of the river Tiber. With time, due to deposition of sediments from the river, the shoreline migrated southwards. Although the earliest human activities in the area date back to 1400-1000 BC, there is a legend that Ostia was founded in the late seventh century BC by the fourth king of Rome, Ancus Marcius. However, the oldest archaeological remains so far discovered date back to the fourth century BC. The vast majority of the excavated buildings are from the first to second centuries AD, which represent the period of most active developments in ancient Ostia during the reign of Trajan, Hadrian and Antoninus Pius. The decline of the city began arguably in the third century AD, followed by episodes of short-term revival, and final abandonment in the ninth century AD.

Most of the ruins of Ostia were excavated in the nineteenth and the first half of the twentieth centuries. At the end of the 1990s, non-invasive geophysical surveys were conducted by the German Archeological Institute (DAI) and the American Academy in Rome (AAR), led by Michael Heinzelmann and Archer Martin. In the early 2000s, the British School at Rome (BSR) and several UK universities on behalf of DAI and AAR also conducted geophysical surveys in different parts of Ostia. These and later studies, primarily involving electrical resistivity and magnetometry surveys, provided a wealth of information about the unexcavated areas of Ostia, which led to important discoveries. More recently, integrated geophysical surveys were performed in Ostia's river harbour, located close to the Tiber to the west of the excavated centre of ancient Ostia (Wunderlich *et al.* 2018a). This study involved electrical resistivity tomography (ERT), ground-penetrating radar (GPR), inversion of surface
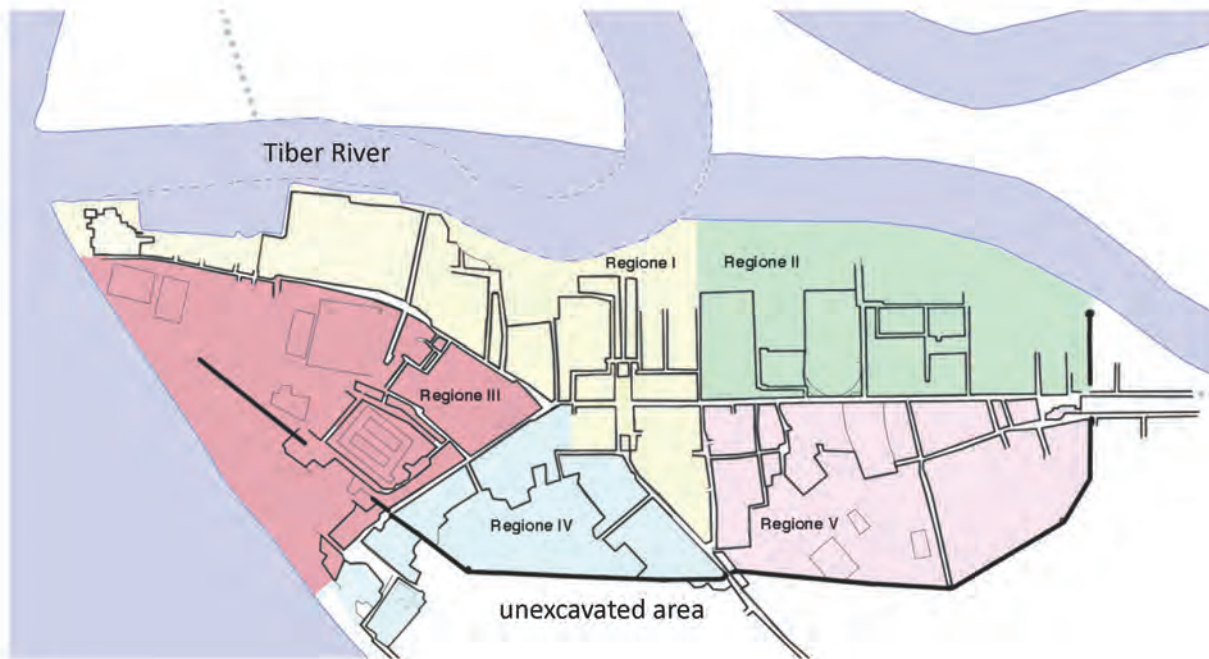
Fig. 4.1 Regions of ancient Ostia (adapted from Consoli 2013). The unexcavated area in the south, where the present study was carried out, is marked

(Love) wave dispersion curves using the MASW (multi-channel analysis of surface waves) method, and refraction tomography using compressional (longitudinal) seismic waves. They detected a low-high-low-high seismic velocity distribution with depth in this area. The very shallow high-velocity layer sandwiched between low velocities was attributed to a deposit that probably resulted from a past tsunami. Wunderlich *et al.* (2018b) succeeded in increasing the resolution and reliability of ERT in Ostia's silted riverbed through constraining the ERT inversion using additional direct push electrical conductivity and vibracore data.

In 2017 we performed high-resolution shear-wave (transverse-wave) seismic reflection surveys for the first time in the unexcavated area located south of Region IV (*Insula* iv) of ancient Ostia (Fig. 4.1). The southern boundary of this region coincides with the southern limit of the excavated area of the ancient city. In the conventional archaeological interpretation of Ostia, which is largely conditioned by the "visible" (excavated) city, the perceived expanse of the city is usually influenced by the extent of the excavation.

As far as Region IV is concerned, its edge has been considered to be the fringe of the built-up area and thus lacking a "visible" neighbourhood on the southern side (Stöger 2011, 68). However, as has been revealed in earlier geophysical surveys, the excavated area of Ostia possibly constitutes only about one third of the city, comprising merely the central areas, while the larger part, including the outlying zones, remains unexcavated (Bauer & Heinzelmann 1999). The goal of the geophysical surveys that we carried out in 2017 was to perform a preliminary search for near-surface seismic scatterers that might indicate the presence of buried structures in this unexcavated field lying outside the southern fringe of the excavated Region IV. Since the expected depth of any buried archaeological structures/objects was very shallow, the focus was to extend the usual limit in order to locate ultra-shallow (less than 2-3 m in depth) structures, thus requiring very close receiver separation, very short seismic wavelength, and the ability to see below the surface-wave trains that typically dominate the near-offset seismic data. In this article we present the first results of the high-resolution shear-wave seismic reflection survey carried out along two profile lines.

We also conducted ERT and GPR surveys at several locations in this site (*e.g.*, Ngan-Tillard *et al.* 2020). The data quality of the ERT surveys was relatively poor and/or lacking resolution (as in Wunderlich *et al.* 2018a who explored Ostia's river harbour area) and the depth of penetration for the GPR surveys in and around this location was limited (see also Locicero & Sonnemann, 2020), possibly due to the presence of topsoil of high electrical conductivity. In antiquity, the sea was the western border of the plain (Pianabella) located to the south of present-day Ostia. The shore migrated gradually to the west (*e.g.* Bradford 1957). As the sea-shore was closer to our test-site in the past than it is now and also due to flood deposits of the river Tiber over the centuries, the saltiness of the topsoil and the high electrical conductivity at shallow depths in this part can be explained.

4.2 ULTRA-SHALLOW SHEAR-WAVE REFLECTION SURVEYS IN OSTIA

Propagating seismic waves sense the distribution of the mechanical properties of the subsoil given by the elastic moduli and bulk density which, in turn, are functions of different soil-physical properties such as porosity, stiffness, compressibility, fluid saturation, suction, degree of compaction, stress, certain pore-fluid properties, etc. In unsaturated or partially saturated, porous, near-surface soils, the velocity of seismic shear waves is much lower than that of seismic compressional waves. As a result, for comparable frequencies one can achieve much shorter wavelength and hence much higher resolution using shear waves than using compressional waves. Secondly, shear waves are directly sensitive to the rigidity of the soil or the underground buried objects, which is an important consideration in the search for a buried archaeological target. Third, shear waves sense the subtle changes in soil types (*e.g.* Ghose & Goudswaard 2004). These are the primary reasons why we chose to use seismic shear waves in our work. Substantial research in the past resulted in the development of high-frequency electromagnetic vibratory sources for high-resolution near-surface imaging (Ghose *et al.* 1996; 1998). In order to generate relatively high frequencies, in Ostia we used as source the electromagnetic shear-wave vibrator (Ghose *et al.* 1996; Ghose 2012).

In 2017 we acquired high-resolution shear-wave reflection data along two lines located in/adjacent to an unexcavated field lying outside the southern limit of the excavated Region IV of the archaeological site of ancient Ostia (Fig. 4.1). Figure 4.2(a) shows the location of the site in an aerial map. In the north, west and north-east of this site the archaeological excavations are visible. The orientations of Line A and Line B are illustrated in Figure 4.2(b). Line A is about 35 m long. Although presently covered with soil, part of this line was excavated in the past, and the distribution of ancient walls and the location of a tumulus just outside the southern limit of Region IV are known from archive photographs. The function of such a tumulus in ancient times remains under discussion. Seismic refraction and tomography mostly using P waves were employed in some past studies to locate buried tombs (e.g., Tsokas *et al.*, 1995; Polymenakos *et al.*, 2004). The goal of our survey along Line A was to check whether a tumulus - located at a very shallow depth (less than 1 m) - could be traced in seismic reflection and scattering data. Line B, about 54 m long, crossed Line A, and then extended to the unexcavated field to the south-west. Line B crossed an earthen road. Based on excavations performed in the nineteenth and twentieth centuries, it is believed that ancient north-west south-east trending streets possibly existed under the unexcavated fields (Bakker 1999). The earthen road crossed by Line B might mark the trail of an important Roman street. The exact course of the street and its intersections with other streets cannot yet be securely established (Stöger 2011).

The field was mostly vegetation- or grass-covered, except near the earthen road where it was dry, compact soil mixed with stone chips. The minimum distance of our seismic lines from the nearest visible, ancient man-made constructions/walls was over 6 m (except for the wall at the end of Line A). This distance was even greater for Line B. This was carefully chosen in order to minimise the interference of side reflections from these structures with reflections from the shallow underground targets (max 3-4 m depth). Any reflection from the wall at the end of Line A showed up as a negative velocity event and could, therefore, be filtered out easily.
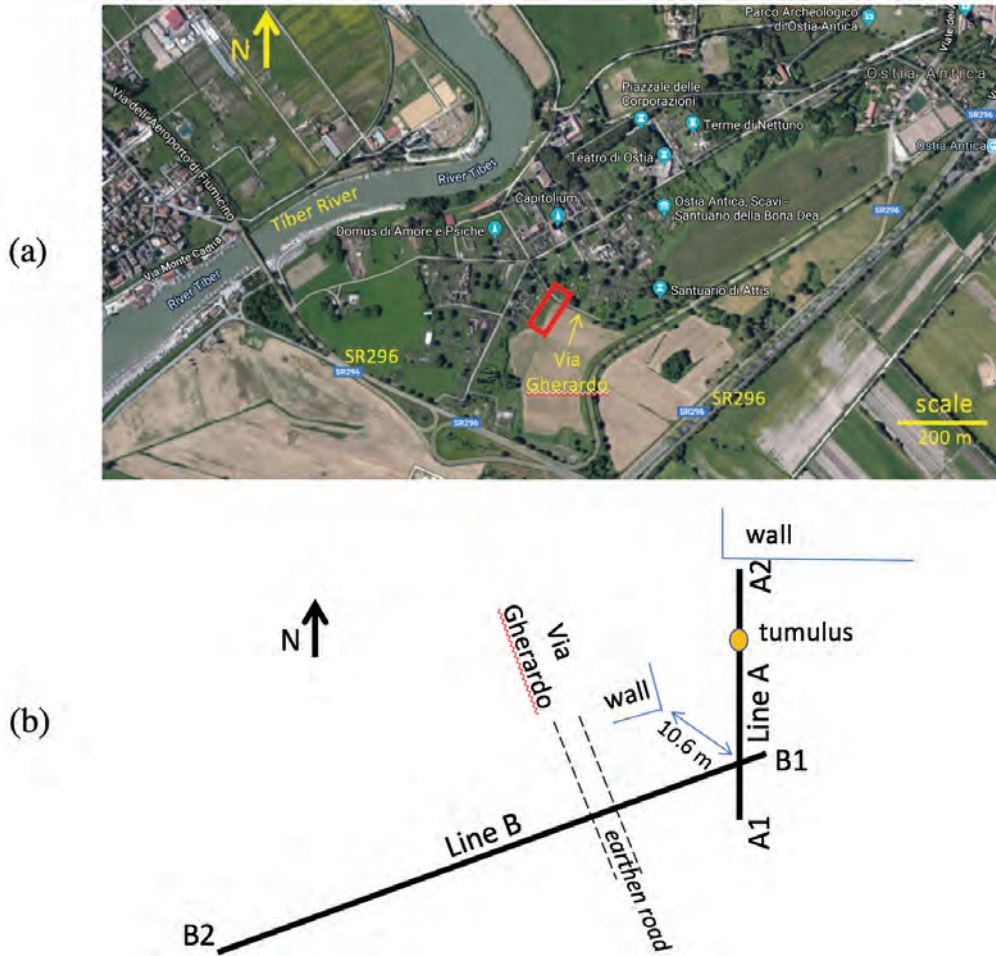
Fig. 4.2 (a) Google map showing an aerial view of ancient Ostia and the River Tiber. The red rectangular area represents the test site for the present study. SR296, the motorway to Fiumicino airport via Ostia, is situated in the south and the east of the test site. (b) The orientation of seismic Lines A and B with respect to the earthen road along Via Gherardo (see Google map). The known location of a tumulus on Line A is marked

Single-component (horizontal crossline orientation) geophones with 10 Hz natural frequency were planted at 25 cm interval (Fig. 4.3). The total number of active geophones per shot was 120. The seismic source (electromagnetic shear-wave vibrator oriented in the crossline direction) was moved by 1 m each time. We used a roll-along mode for data acquisition. When the source moved by 24 receiver stations, the first cable (of 24 channels) was moved to the end, and the data acquisition continued. At the beginning of shooting every line, the acquisition geometry was inline end-on, but later on it changed to split-spread. At the end

of shooting a line, the geophones were kept fixed; only the source moved. The data were sampled at 1 kHz Nyquist frequency. We fed a non-linear sweep to the electromagnetic vibrator to acquire very high-frequency shear-wave data. Multiple accelerometers placed on the vibrator (on baseplate and reaction-mass) were used to calculate the groundforce signal for each source separately, which was then used to compress the raw vibrograms (Ghose 2002).

Along and adjacent to our seismic Line A, ancient structures and the tumulus can be marked in an
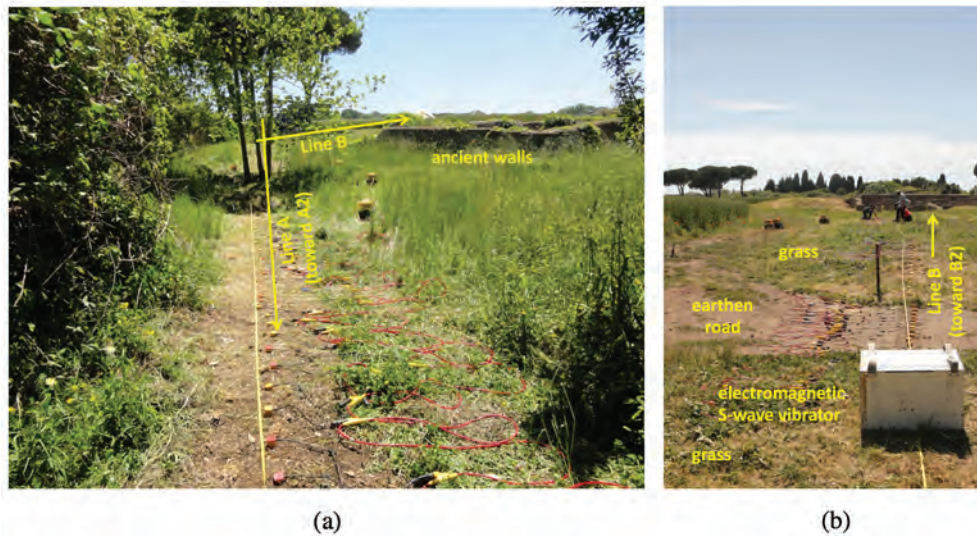
Fig. 4.3 The ground surface and vegetation condition along Lines A and B. Crossline-oriented, horizontal geophones planted at 25 cm interval and the electromagnetic shear-wave vibrator source are visible

archive photograph (Fig. 4.4). All these structures are now covered by 0.5-2 m thick soil. Near the tumulus the elevation of the ground reaches its minimum.

Figure 4.5 shows representative common-source (shot) gathers for seismic lines A and B (field-file ID or FFID 18, 13 and 63 for Line A and FFID 9, 77, 87 for Line B). These gathers are compressed, raw shot gathers - after only trace editing (dead trace elimination and correction for reverse traces). The lateral distance (in m) of the common midpoint (CMP) is marked in the horizontal axis. The elevation with respect to the mean sea level is plotted above each shot gather. The predominant frequency for the observed shear-wave reflections/scattering in these shot gathers is 80-100 Hz (time period 10.0-12.5 ms). The surface condition along Line A changes quite rapidly; this can be seen in the sharp changes in the lateral appearance and continuity of the surface waves in the shot gathers in Figure 4.5(a). The data are somewhat noisy due to the wind-driven movement of nearby vegetation and suboptimal geophone coupling due to the hard condition of the topsoil. Nevertheless, hyperbolic reflection events from geological layer boundaries (yellow arrows) and localised diffractions, probably
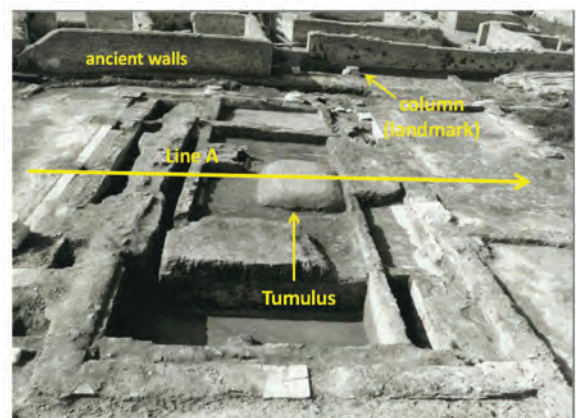
Fig. 4.4 An archive photograph showing the tumulus and the surrounding ancient structures, all of which (except the walls and the column in the upper part of the photograph) are now buried under soil cover. The orientation of the seismic Line A is indicated

from shallow heterogeneities/objects (short vertical red arrows), are identifiable in the raw shot gathers. Interestingly, we notice in Figure 4.5(a) close to CMP_X=24 m that there is an occurrence of strong back-scattered energy. This CMP_X location corresponds to the known location of the mysterious

55
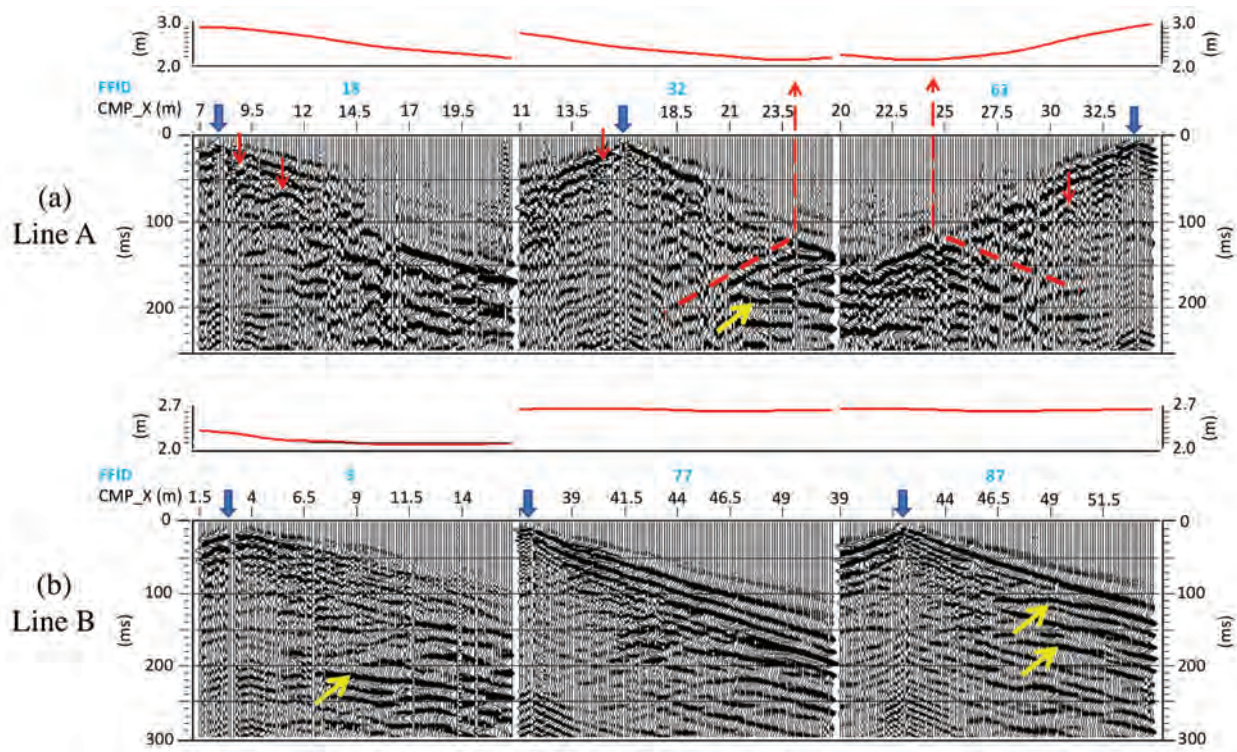
Fig. 4.5 120-channel, common-source (shot) gathers, representing (a) Line A and (b) Line B. Above each shot gather, the red line indicates the elevation at the receiver location. The horizontal axis is the lateral distance/location in CMP_X (m). The vertical axis is two-way time (ms). The thick blue arrow in the top margin of each shot gather indicates the source location. The yellow arrows mark some reflection events corresponding to geological layer boundaries. The small vertical red arrows indicate some shallow scatterers. The red dashed line shows back-scattered energy from approximately CMP_X = 25 m, which matches well with the known location of the tumulus

tumulus of Roman time. From the frequency content and strength, this back-scattered event appears to be primarily a surface wave. The red-dashed lines in Figure 4.5(a) indicate that this location corresponds to the point of least elevation along seismic Line A.

The data are relatively less noisy in the case of Line B. Compared to Line A, in Line B - which passes mostly through the unexcavated part of the field - the surface condition is relatively homogeneous, except in the beginning and where the line crosses the earthen road. We indeed notice in Figure 4.5(b) more continuous alignment of surface waves and other events in FFID 77 and 87 and somewhat less continuity in FFID 9.

4.3 DATA PROCESSING AND INTERPRETATION

In the search for ultra-shallow, shear-wave scatterers of potential archaeological significance it is important that the processing of seismic reflections be kept at a bare minimum - not to lose the subtle signature of a very shallow, buried target. We performed trace editing (trace kill and trace reverse), elevation static and geometrical-spreading corrections (using 180 m/s velocity) and band-pass (10-110 Hz) filtering. This was followed by CMP sorting, velocity analysis, NMO correction and CMP stacking. Post-stack data were subjected to predictive deconvolution, spectral shaping and automatic gain correction (AGC). Because the goal was to locate the ultra-shallow
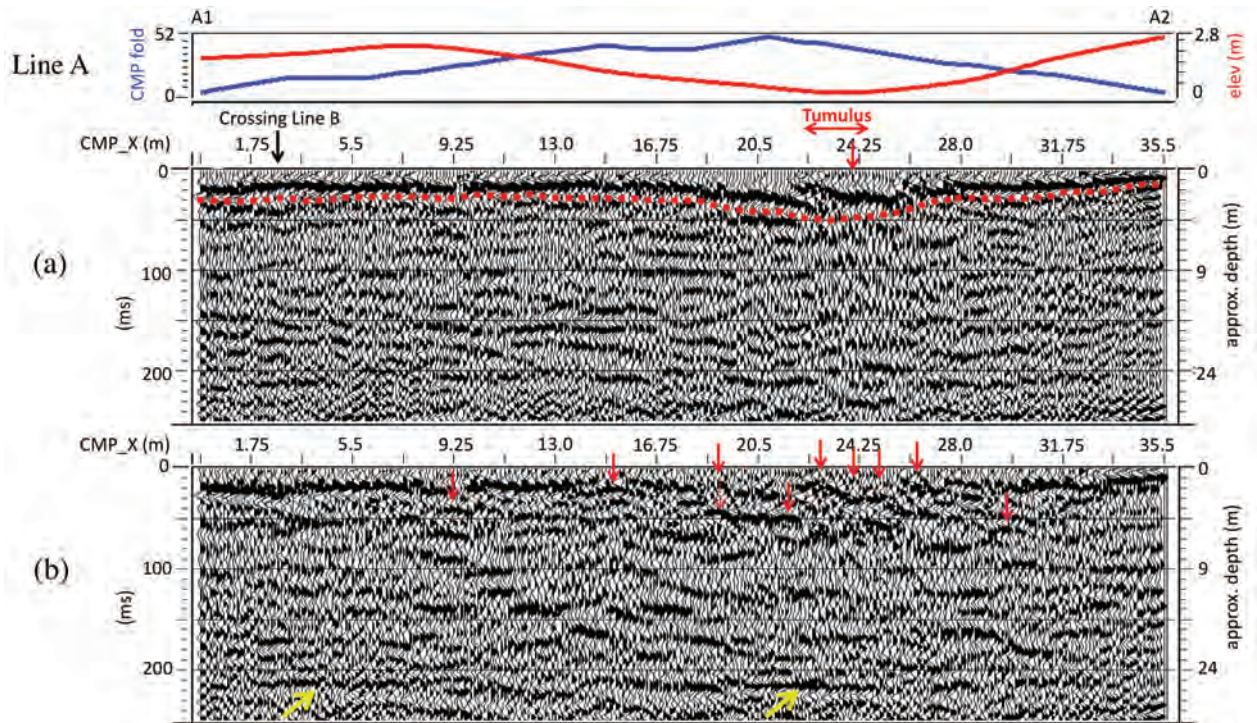
Fig. 4.6 Stacked section for Line A (the points A1 and A2 are shown in Figure 4.2(b)). (a) A constant stacking velocity that stacks primarily the surface waves was used. Note that the trend of the surface wave alignment matches with that of the elevation plotted with a solid red line in the top. (b) Stacked section using a 1-D stacking velocity field which minimises the stacked surface-wave energy. Note that still some surface wave remains in (b). However, some body-wave scatterers have become more visible in (b). The small red arrows in both figures mark localised diffraction patterns (scatterers), some of which might correspond to the location of shallow underground objects. The yellow arrows indicate shear-wave reflections from geological layer boundaries

scatterers, it was not an option to remove the surface waves through muting. The frequency-wavenumber (*f-k*) filtering did not work, as the velocity of the surface waves and that of the shallow reflections or the scattered events were too close to each other.

To be able to identify body-wave scatterers present below the stacked surface waves, at first a stacking velocity of 135 m/s was found to maximise the surface waves in the stacked section corresponding to Line A, as shown in Figure 4.6(a). Here, the alignment of surface waves is marked by the red-dashed line. In the upper part of Figure 4.6, the elevation (red line) and the CMP stack fold (blue line) are plotted as functions of lateral distance (CMP_X). Note that

the alignment of surface waves in the stacked section follows the surface elevation, which is explicable. In the next step, velocity analysis was carried out and a depth-varying (1-D) velocity field was estimated that minimised the surface-wave energy in the stacked data, shown in Figure 4.6(b). Some surface-wave energy still remained in the data. Nevertheless, through comparison of Figure 4.6(b) with Figure 4.6(a), it is possible to interpret with reasonable confidence several shallow scatterers, as marked by red arrows in Figure 4.6(b) and one also in Figure 4.6(a) located around 24 m CMP_X. The body-wave scatterers do not co-locate and match in spatial trend with the predominant surface waves. The scatterer marked around 24 m CMP_X is very likely to be
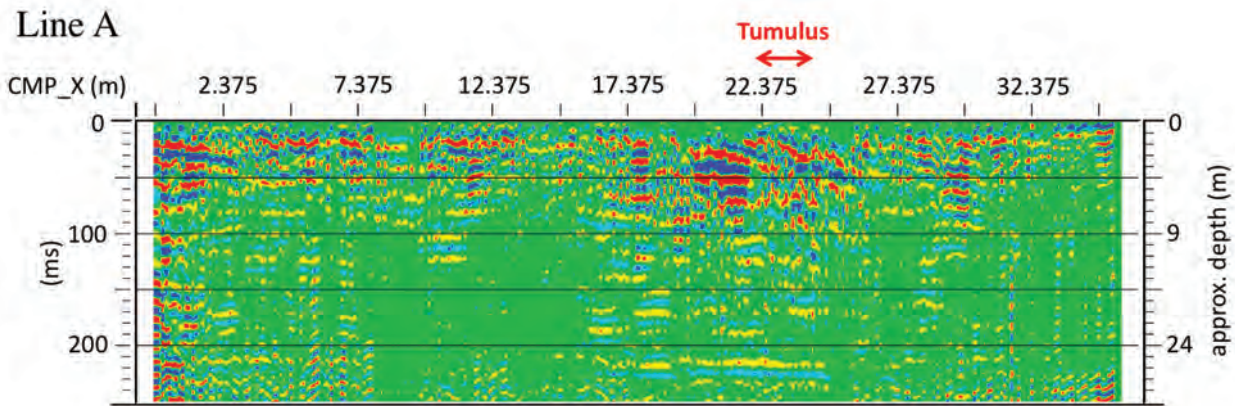
Fig. 4.7 Amplitude of seismic events in the stacked section in Figure 4.6(b), without AGC and spectral shaping

caused by the shallow, buried tumulus. Several other plausible scatterers are marked in Figure 4.6(b). The yellow arrows in Figure 4.6(b) indicate geological layer interfaces. The stacking velocity field that produced Figure 4.6(b) had a lower stacking velocity (V_stack=125 m/s) between 50 and 200 ms two-way time than at earlier times (V_stack=250 m/s) and at later times (V_stack=350 m/s). The presence of such seismic velocity reversal was earlier reported by Wunderlich *et al.* (2018a) in the harbour area of Ostia, situated to the west of the present location.

Next, we looked at the intensity of scattering. The magnitude of the scattered energy depends on the impedance contrast at the point of scattering. From a denser and stiffer object the intensity of the back-scattered energy would be higher than that from a softer object. In Figure 4.7, a true-amplitude stacked section (i.e., one without application of spectral shaping and AGC) corresponding to Figure 4.6(b) shows the scattered-intensity distribution. Note that the scattered intensity is high near the location of the tumulus and slightly left of this location. The tumulus is made of hard material/stone, which back-scatters more seismic energy than the surrounding area. Figure 4.4 shows in archive photograph this seismic line with respect to the location of the tumulus. We can spot the presence of prominent building structures to the left of the tumulus. This evidence serves as ground truth for the interpretation of the seismic events.

Figure 4.8(a) shows the stacked section for Line B, where the surface-wave energy is predominantly accentuated. A constant stacking velocity of 200 m/s was used. The topsoil here was more compact than along Line A, which might explain the higher stacking velocity than for the section in Figure 4.6(a). The alignment of surface waves is indicated by the red-dashed line in Figure 4.8(a). It is evident that this alignment follows the elevation at this site, as illustrated in the upper plot. The indication of some very shallow scatterers is present, but not very clear in Figure 4.8(a). Next, an average 1-D velocity field was estimated that minimises the surface-wave energy in the stacked section. The resulting stacked section is shown in Figure 4.8(b). The yellow arrows in Figure 4.8(b) mark reflections from geological layer boundaries. From a comparison of Figure 4.8(b) with Figure 4.8(a), the presence of several localised diffraction patterns is clear; these are indicated by the red arrows in Figure 4.8(b). The depth-varying velocity field (two-way time: velocity function) that was used to produce the stacked section in Figure 4.8(b) is as follows: 0 ms: 200 m/s; 50 ms: 150 m/s; 200 ms: 250 m/s. In addition to the very shallow diffractors, in Figure 4.8(b) some relatively deeper heterogeneities also generating diffracted waves are visible. Because the shallow diffractors are considerably localised and small (for the seismic wavelength used), it is not advisable to migrate the seismic data, as that will focus the diffracted energy into a restricted region and make identification of these diffractors difficult.
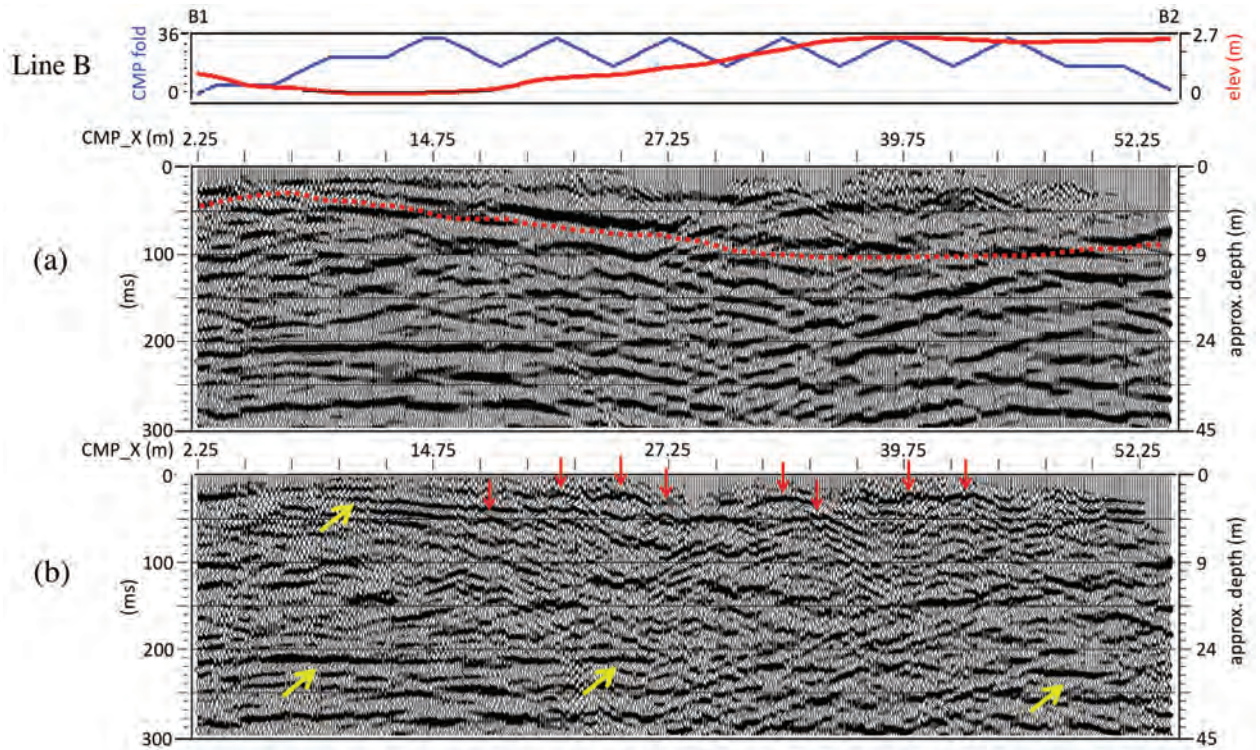
Fig. 4.8 Stacked section for Line B (the points B1 and B2 are shown in Figure 4.2(b)). (a) A constant stacking velocity was used to stack primarily the surface waves. The trend of the aligned surface waves matches remarkably with that of the elevation plotted in the top. (b) Stacked section using a 1-D stacking velocity field which minimises the stacked surface-wave energy. Several body-wave scatterers have become much clearer in (b). The small red and yellow arrows mark the same as in Fig. 4.6
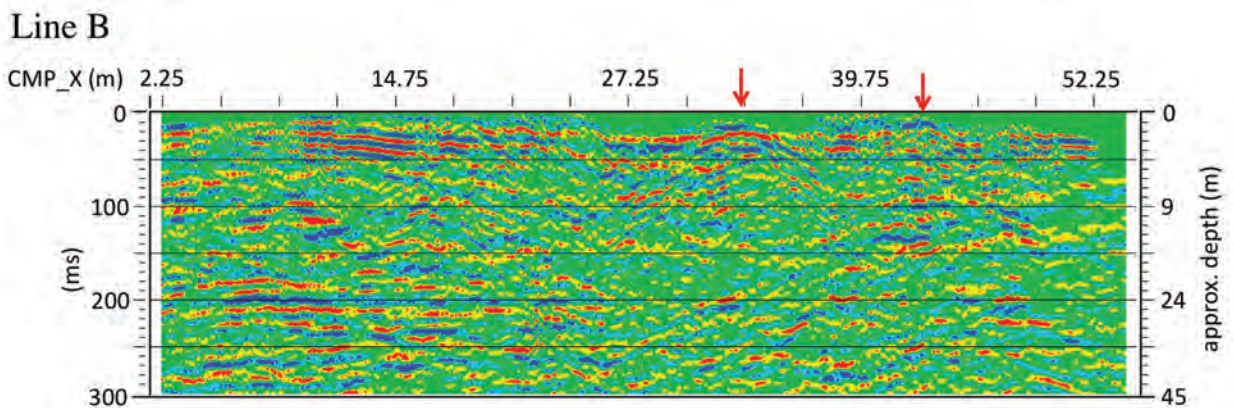
Fig. 4.9 Amplitude of seismic events in the stacked section in Figure 4.8(b), without AGC and spectral shaping. The red arrows mark some prominent scatterers
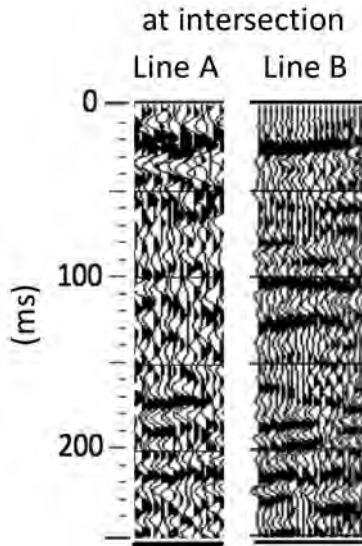
Fig. 4.10 The match between the two stacked seismic sections (Figures 4.6(b) and 4.8(b)) at their intersection point. The CMP stack fold and the signal-to-noise ratio are different between the two datasets. Note that the main reflection events coincide in time between the two lines

Figure 4.9 shows the true-amplitude stacked section corresponding to Figure 4.8(b). The intensity of scattering is very high for the scatterer located at CMP_X around 32 m, marked by the red arrow in Figure 4.9. This might be the location of a buried object of a significantly higher density than its surroundings. Another strong scatterer is located at around 42.5 m, also marked in Figure 4.9.

In Figure 4.10, parts of the seismic sections at the intersection of two lines, Line A and Line B, are plotted next to each other. Data along these two profiles were acquired independently, the receiver-coupling conditions and the noise levels were different, and the processing was done independently for the two sections. We note that the main reflection events in the two sections appear generally at the same two-way time.

4.4 DISCUSSION

In Figures 4.6-4.10, the approximate depths derived from the stacking velocity field are indicated on the right hand side. For the detected ultra-shallow scatterers, the seismic wavelength that we note in the data is about 1 m, which implies a resolution of roughly 25 cm. Such a high resolution could be achieved through use of shear waves in combination with the high-frequency electromagnetic vibrator generating non-linear sweep signals. Because it is a relatively small and non-invasive source, it is suitable for use in an archaeological site like Ostia. Such a high resolution might be challenging in conventional surveys using MASW or ERT surveys.

Our results illustrate that the use of high-frequency shear waves is quite promising for localising the back-scattered energy from shallow archaeological objects. In this pilot study the goal was to investigate this possibility. In this regard, our investigation has achieved its goal and has provided valuable insights into specific aspects where care should be taken. In a more complete archaeological investigation it will be crucial to do not 2-D but 3-D high-resolution, shear-wave seismic reflection surveys in order to localise the scatterers more accurately in space. Removal or suppression of surface waves is crucial to the illumination of shallow, body-wave scatterers. Recently, a data-driven approach combining seismic interferometry with adaptive subtraction of surface waves has been developed and tested successfully on field data (Konstantaki *et al.* 2015; Liu *et al.* 2018; 2019). It will be useful to develop this approach further to reliably image the very shallow scatterers like the ones that we detected in Ostia in this study. Also reverse-time migration and full-waveform inversion could be powerful tools for localising such shallow scatterers. Our results indicate that, for archaeological site investigation, shear-wave seismic reflections can provide a high-resolution complementary method to more conventional ERT, GPR and magnetometry surveys.

4.5 CONCLUSIONS

We have presented the first results of a high-resolution shear-wave seismic reflection survey carried out along two profiles – Line A and Line B - in the unexcavated area south of Region IV (*Insula* iv) of ancient Ostia. One important goal was to check whether the relatively low-lying southern fields present any indication of the presence of shallow-buried (at a depth of less than 2-3 m) objects, which will have important implications on the extent of the urban development and social activities in the ancient Roman harbour city of Ostia. Our results illustrate that the use of high-frequency shear waves is quite promising for localising the back-scattered energy from shallow-buried archaeological objects. We have found very distinct scattered shear-wave energy from a mysterious tumulus whose location along Line A was known. It was possible to interpret with reasonable confidence the location of several conspicuous, shallow scatterers in both Line A and Line B. The use of shear waves and a high-frequency, electromagnetic shear-wave vibrator was crucial in order to achieve a seismic wavelength of about 1 m and hence a resolution of about 25 cm. The suppression of surface waves is crucial to the illumination of the shallow scatterers/objects. Also, the intensity of the back-scattered energy can be informative about the hardness or density of a buried scatterer. In the future, to localise and image the shallow archaeological objects more reliably the use of 3-D shear-wave seismic reflection, in combination with new data processing and analysis approaches like seismic interferometry, full-waveform inversion, and reverse-time migration, appears very promising.

References
Bakker, J.T. 1999. A topographical dictionary of Ostia. https://www.ostia-antica.org/dict.htm

Bauer, F.A. & Heinzelmann, M. 1999. The Constantinian Bishop's Church at Ostia: preliminary report on the 1998 season. *Journal of Roman Archaeology* 12, 342-353

Bradford, J. 1957. *Ancient Landscapes: Studies in Field Archaeology.* London: G. Bell and Sons

Consoli, R., 2013. Ostia. *Ancient History Encyclopedia*. Retrieved from https://www.ancient.eu/Ostia/

Ghose, R. 2002. High-frequency shear wave reflections from shallow subsoil layers using a vibrator source: Sweep cross-correlation versus deconvolution with groundforce derivative. *Extended Abstract, SEG Annual Conference*, 408-1411

Ghose, R. 2012. A microelectromechanical system digital 3C array seismic cone penetrometer, *Geophysics* 77(3), P. WA99-WA107

Ghose, R., Brouwer, J. & Nijhof, V. 1996. A portable S-wave vibrator for high-resolution imaging of the shallow subsurface. *Extended Abstract, 58th EAGE Conference and Exhibition*

Ghose, R, Nijhof, V., Brouwer, J., Matsubara, Y., Kaida, Y. & Takahashi, T. 1998. Shallow to very shallow high resolution seismic imaging using a portable vibrator system. *Geophysics* 63, 1295-1298

Ghose, R. & Goudswaard, J. 2004. Integrating S-wave seismic-reflection data and cone penetration test data using a multiangle multiscale approach. *Geophysics* 69(2), 440–459

Konstantaki, L.A., Draganov, D., Ghose, R. & Heimovaara, T. 2015. Seismic interferometry as a tool for improved imaging of the heterogeneities in the body of a landfill. *Journal of Applied Geophysics* 122, 28-39

Liu, J., Draganov, D. & Ghose, R. 2018. Seismic interferometry facilitating the imaging of shallow shear-wave reflections hidden beneath surface waves. *Near Surface Geophysics* 16(3), 372- 382

Liu, J., Bourgeois, Q., Ghose, R. & Draganov, D. 2019. Detection of near-surface heterogeneities at archaeological sites using seismic diffractions. *First Break* 37, 107-111

Locicero, M.A. & Sonnemann, T. 2020. Behind the Block: results from a geophysical study of the unexcavated area in the southwest of Ostia. In H. Kamermans & L.B van der Meer (eds),

Designating Place. Archaeological Perspectives on Built Environments in Ostia and Pompeii. Archaeological Studies Leiden University 50. Leiden: Leiden University Press

Ngan-Tillard, D., Draganov, D., Warnaar, M., Liu, J., Brackenhoff, J., Berg, J. van den, Veltmeijer, A. & Stöger, H. 2020. Exploring with GPR the frigidarium of the Byzantine baths in Ostia Antica after excavation, backfilling and floor retiling. In H. Kamermans & L.B. van der Meer (eds), *Designating place: archaeological perspectives on built environments in Ostia and Pompeii.* Archaeological Studies Leiden University 50. Leiden: Leiden University Press

Polymenakos, L., Papamarinopoulos, S., Liossis, A. & Koukouli-Chryssanthaki, C. 2004. Investigation of a monumental Macedonian tumulus by three-dimensional seismic tomography. *Archaeological Prospection* 11(3), 145-158

Stöger, H. 2011. *Rethinking Ostia: A Spatial Enquiry into the Urban Society of Rome's Imperial Port-Town*. Archaeological Studies Leiden University 24. Leiden: Leiden University Press

Tsokas, G.N., Papazachos, C.B., Vafidis, A., Loukoyiannakis, M.Z., Vargemezis, G. & Tzimeas, K. 1995. The detection of monumental tombs buried in tumuli by seismic refraction, *Geophysics* 60(6), 1735-1742

Wunderlich, T., Wilken, D., Erkul, E., Rabbel, W., Vött, A., Fischer, P., Hadler, H. & Heinzelmann, M. 2018a. The river harbor of Ostia Antica – stratigraphy, extent and harbor infrastructure from combined geophysical measurements and drillings. *Quaternary International* 473, 55-65

Wunderlich, T., Fischer, P., Wilken, D., Hadler, H., Erkul, E., Mecking, R., Gunther, T., Heinzelmann, M., Vött, A. & Rabbel, W. 2018b. Constraining electrical resistivity tomography by direct push electric conductivity logs and vibracores: An exemplary study of the Fiume Morto silted riverbed (Ostia Antica, western Italy), *Geophysics* 83(3), B87-B103